

Chapter 1

Introduction

This thesis is a study of a relatively cold partially ionized component in the interstellar medium using observations of very low frequency (**30–1420 MHz**) recombination lines of carbon. In this opening chapter, we present a brief overview of the interstellar medium, a short review of radio recombination lines and finally a preview of the present work.

1.1 The Interstellar Medium (ISM) - an Overview

The space **between** stars in the **Galaxy** is filled with gas containing hydrogen, helium, oxygen, carbon, calcium, and many other elements and dust grains. This constitutes the interstellar medium (ISM). The ISM is observed to **be** highly inhomogeneous with most of the mass being concentrated in clouds, both atomic and molecular, which occupy a small fraction of the volume in the Galaxy. The rest of the volume is filled by a warmer all-pervading intercloud gas. Matter in some parts of the ISM condense to form stars. In other parts, stars explode as supernovae, thus returning matter back to the ISM, and enriching it in heavier elements which are synthesized inside the stars. Thus, the ISM is a dynamic system in the Galaxy in which there is a constant exchange of matter and energy between its different components and also between it and the stars. The energetics of the ISM are governed mainly by the mass exchange between massive stars and the ISM. The low-mass stars, because of their low level of activity and their final essentially inactive state, do not return much of their mass to the ISM and instead gradually deplete the ISM of its gas and dust.

Hydrogen is the most abundant species in the Galaxy - both in the ISM and in stars. Helium comes next with a cosmic abundance of **0.1** by number, if the abundance of hydrogen is one. Carbon has a cosmic abundance by **number** of about 3×10^{-4} on **the** same scale and is the fourth abundant element after oxygen. The abundance of all other elements are much less **than** that of carbon. Hydrogen and other elements are

observed in ionized, atomic and molecular forms.

1.1.1 Classification of the ISM based on the dominant form of Hydrogen

Ionized Clouds:

All the hydrogen in the vicinity of hot O & B stars where the ultraviolet flux (with $\lambda < 912\text{\AA}$) is intense, exists in ionized form known as H II regions. Helium, which has a first ionization potential = 24.4 eV is also expected to be singly ionized close to the O & B stars whereas carbon with a second ionization potential = 24.4 eV is likely to be doubly ionized. While the electrons that are freed in the ionization process provide the heating in this region, collisionally-excited forbidden lines of oxygen and other heavier elements act as the cooling agents. These heating and cooling processes establish equilibrium temperatures in these regions in the range $(5-10) \times 10^3$ K whereas the electron densities range from 10 to 10^4 cm^{-3} . Recombination of electrons with ions is the inverse process, which balances the process of ionization. If an electron recombines to an excited state, then recombination lines are emitted as the electron cascades down to the ground state. The Balmer H α , H β and higher-frequency ($\nu > 1 \text{ GHz}$) radio recombination lines of hydrogen are readily observed from H II regions. These ionized regions are not in pressure equilibrium with the ISM; because of high-pressure these regions expand into the surrounding medium. The density inhomogeneities in the surrounding gas forces the ionized gas to channel out asymmetrically in some cases. Most of the Galactic H II regions are density-bounded and the residual stellar ultraviolet flux ionizes the low-density ambient medium. In Fig 1.1, we show the radial distribution of ionized hydrogen in the Galactic disk. Ionized gas shows a peak in the surface density in the range 3 – 7 kpc from the Galactic centre, which is similar to the distribution of molecular hydrogen (H₂).

Atomic Clouds:

More than 95 % of the mass in the ISM is in the form of neutral hydrogen (almost equal mass in atomic and molecular forms) and helium. Atomic hydrogen (HI) is thus an important phase of the ISM. This form of hydrogen is extensively studied using the 21-cm line which arises due to transition between the hyperfine levels in its ground state. The 21 cm line has been observed in emission and absorption throughout the Galaxy. Wide emission lines are observed from all directions in the Galaxy, whereas narrow absorption lines are observed towards background galactic and extragalactic continuum sources.

Chapter 1

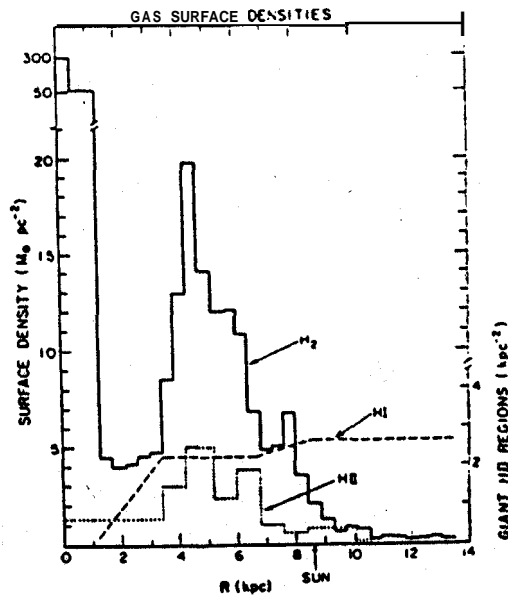


Figure 1.1 Comparison of gas surface densities in the Galactic disk. Value of H_2 (Clemens, Sanders & Scoville 1988) and HI (Burton & Gordon 1978) include a 1.38 correction factor for He and they have been scaled to $R_0 = 8.5$ kpc. The figure is taken from Scoville (1990)

The HI gas is all-pervasive and its radial distribution in the Galaxy is distinct from that of ionized and molecular gas (See Fig 1.1). As shown in Fig 1.1, except for a decrease in the surface density near the Galactic centre, the radial distribution of HI in the Galaxy is almost uniform. The primary heating mechanism in the atomic gas are the photoelectrons from dust grains whereas the cooling is due to the collisionally-excited fine structure lines of [CII] (158 μm line), CI (370 μm & 609 μm lines) and [OI](63 μm & 145 μm). Regions of predominantly atomic hydrogen have temperatures ranging from 30–8000 K and a wide range of densities. These different components are in pressure equilibrium with typical pressures P/k (where $P=nkT$ is the gas equation) of $\sim 4000 \text{ cm}^{-3} \text{ K}$. HI gas exists in the form of discrete clouds as well as a diffuse component pervading the entire galaxy.

Molecular Clouds:

Molecular clouds are the densest regions of the ISM and star formation activity is associated with them. Much of the molecular gas appears in the form of giant molecular clouds (GMC) which are self-gravitating. The pressure in these clouds is much larger than the thermal pressure observed in the diffuse ISM. As shown in Figure 1.1, the gas

surface density of molecular hydrogen exceeds that of atomic and ionized hydrogen in the central regions of the Galaxy. There is a steep rise in the surface density of molecular gas in the central **500 pc** of the Galaxy and in a ring of galactocentric radii between **3–7 kpc** (Scoville & Solomon **1975** & Burton *et.al.* **1975**). More than **65** molecules and their isotopic variants have been found to reside in molecular clouds. Typical temperatures in molecular clouds is **10 – 20 K** which **is** the expected equilibrium temperature for a balance between heating by low-energy **cosmic** rays and cooling-by the rotational transitions in carbon monoxide. Hydrogen densities in molecular clouds range from 10^3 to 10^6 cm^{-3} .

Hydrogen molecule (H_2) **lacks** a permanent dipole moment and hence there are no permitted rotational transitions which normally occur in the radio or **IR** bands. However, there are allowed electronic transitions in the Lyman and Werner bands in the ultraviolet. Since these cannot be used to probe distant, obscured molecular regions, transitions in other molecules which are **collisionally** excited by the H_2 molecule are used as tracers. **One** such widely used molecule is **CO**. ^{12}CO has observable rotational transitions (*e.g.* **J=1-0** and **J=2-1**) in the radio band, which are collisionally excited by H_2 molecules. In addition other molecules, such as **CS**, **HCN**, **NH₃** etc which are excited at higher molecular densities are also used as diagnostics of the properties of molecular clouds.

1.1.2 Pressure Equilibrium in the ISM

As mentioned before, the multi-phase gas filling most of the volume in the Galaxy is observed to be at an average pressure $\sim 4000 \text{ cm}^{-3} \text{ K}$ (McKee & Ostriker **1977**). A theoretical explanation for the existence of this multi-phase behaviour of the **ISM** was first provided by Field, Goldsmith and Habing (**1969**; FGH). They showed that the temperature dependence of the cooling rate of interstellar gas was such that cold ($T \sim 10^2 \text{ K}$), neutral (**HI**) clouds could coexist in pressure equilibrium with warm ($T \sim 10^4 \text{ K}$) intercloud **HI** over a limited range of pressures, close to the pressure observed in the ISM. In their model, the heating was provided **mainly** by low-energy cosmic rays and the cooling by collisional **excitation** of hydrogen and helium at high temperatures and by atoms like C^+ at low temperatures. **FGH** also suggested the possible existence of a third stable phase above a temperature of 10^6 K in which **bremstrahlung** is the chief cooling process. Cox & Smith (**1974**) argued that the supernova explosions in the Galaxy made a network of hot tunnels in the ISM with a filling factor of about **10 %**. Measurements made by the **Copernicus** satellite during **1970-80** using the ultraviolet absorption lines of atomic and molecular hydrogen observed in stellar spectra showed

that the volume density of hydrogen in the ISM varied by two orders of magnitude. These observations highlighted the patchiness of the interstellar gas which had to be considered by models of the interstellar medium. In 1977, McKee & Ostriker put forward a three-component model for the ISM regulated by supernova explosions in an inhomogeneous medium. In their model, the two components of the FGH model were embedded in a third medium whose filling factor was much larger, almost 70 %, and it constituted the background medium. The three components, then make up most of the volume in the Galaxy and are roughly in pressure equilibrium. Although the McKee & Ostriker model may not be applicable in its entirety to the ISM, it does provide a reasonable picture of the various components of the ISM. These are described briefly below:

- **Hot Ionized Medium (HIM):** This component with a typical temperature of 5×10^6 K and electron density of 0.003 cm^{-3} has a filling factor of 0.7 to 0.8 and is also known as the coronal gas. It is observed in soft X-ray emission and in ultraviolet absorption lines of [O V], [NIV], [SIII], [SiIII]. Measurements in the UV made by the Copernicus satellite were instrumental in obtaining information on this component.
- **Cold Neutral Medium (CNM):** Cold, neutral relatively dense clouds embedded in the HIM constitutes the CNM. The filling factor of these clouds in the Galaxy is 0.02 – 0.04 and the atomic density and temperature are of the order of $20 - 50 \text{ cm}^{-3}$ and 30 – 80 K respectively. These clouds are easily observed in absorption studies of HI gas and are confined to regions close to the galactic plane with a scale height ~ 100 pc. The degree of ionization in this gas is not known with certainty (Kulkarni & Heiles 1988). The typical sizes of the clouds are a few parsecs to several tens of parsecs.
- **Warm Neutral & Warm Ionized Medium (WNM & WIM):** Surrounding the cold, neutral clouds is a warm photoionized cloud corona at a temperature close to 8000 K and a filling factor much larger than that of the CNM. The cloud corona is divided into two regions. An outer region known as the warm ionized medium (WIM) where the fractional ionization is about 0.7, maintained by hot (B) stars. This component is observed in diffuse Ha (Reynolds 1984) and pulsar dispersion measurements and its local electron density is inferred to be about 0.25 cm^{-3} . However, the filling factor of this gas is not well-determined although the line of sight averaged electron density is known to be $\sim 0.03 \text{ cm}^{-3}$. An inner layer

of smaller volume which is nearly neutral constitutes the warm neutral medium (WNM). The fractional ionization in this component is not known. WNM is mainly observed in HI emission and the scale height of the gas within the solar circle is ~ 500 pc (Lockman 1984). Because of its high spin temperature ($T \sim 10^4$ K), the component has not been detected in absorption.

The interchange of material between the different phases noted above due to various processes such as cloud evaporation, photoionization etc is quite rapid and the mass in a given volume element typically changes phase in a time less than 10^6 years. The McKee-Ostriker model differed from the FGH model in that 1) it included a third phase which is the HIM and 2) the interstellar thermal pressure is determined by supernova explosions.

In the McKee-Ostriker model, molecular clouds and HII regions are not included since they are not in pressure equilibrium with the other components of the ISM and occupy only a small volume of the Galaxy.

1.1.3 Ionized Carbon in the ISM

Owing to the relatively low first ionization potential of carbon (11.4 eV) and its relatively high abundance ($C/H \sim 3 \times 10^{-4}$), many components of the ISM seem to contain detectable amounts of singly ionized carbon (CII). Carbon can be easily ionized by the background ultraviolet photons. CII regions can be studied using recombination lines of carbon in the radio band and using the [CII] fine-structure line at $158 \mu\text{m}$ in the infrared band. Observations of the $158 \mu\text{m}$ [CII] line have found ionized carbon to be widespread in the Galaxy (Shibai *et.al.* 1991, Shibai *et.al.* 1996, Bennett & Hinshaw, 1993, Heiles 1994). Petuchowski & Bennett (1993) have inferred from the COBE observations that most of the [CII] line emission in the Galaxy originates in the extended low-density warm-ionized medium (ELDWIM). Heiles (1994) has also argued that the probable sites of production of the fine-structure line of carbon in descending order of significance are the ELDWIM, the cold neutral medium (CNM) and the photo-dissociation regions (PDR) which occur in the boundaries between ionized gas and molecular clouds (Tielens & Hollenbach 1985, Hollenbach *et.al.* 1991). This points at the ubiquitous nature of singly-ionized carbon; it is associated with both neutral and ionized hydrogen gas. However, it is not clear under which physical conditions detectable recombination lines of carbon are formed. Theoretical basis for possible correlation between the two lines comes from the importance of dielectronic-like recombination (Watson, Western & Christensen 1980 (hereafter WWC80)) in determining the

populations of high quantum number states in carbon under certain physical conditions. This process involves the excitation of the fine-structure transition, $^2P_{1/2} \rightarrow ^2P_{3/2}$ in singly-ionized carbon which on de-excitation gives rise to the 158 μm line.

1.2 Radio Recombination Lines - A Brief Review

Kardeshev (1959) predicted that radio recombination lines of hydrogen and helium would be observable from ionized gas in the Galaxy. Recombination lines are formed when an excited electron in an atom makes transitions between different energy levels. These lines cover a wide range of frequencies, appearing in ultraviolet (Lyman α , $n = 2 \rightarrow 1$) to long radio wavelengths ($\lambda \sim 15$ m, $n \sim 730$). Kardeshev's prediction was confirmed when Dravskikh & Dravskikh (1964) and Sorochenko & Borozich (1964) at Puschino Observatory reported the first detection of a hydrogen RRL at $\lambda \sim 5.2$ cm ($\text{H}104\alpha$ at 5.763 GHz) from the Omega nebula. Soon after, Hoglund & Mezger (1965) reported the detection of the $\text{H}109\alpha$ line. Palmer *et.al.* (1967) detected the first carbon recombination line from the directions of W3 and NGC2024. Since then, recombination lines of hydrogen, helium and carbon have been detected from a variety of regions. While the lines of hydrogen and helium are detected mostly from hot fully ionized regions, carbon lines are detected in cooler partially ionized regions. Observations of RRLs are useful for several reasons as listed below:

- To determine various physical properties such as temperature, density and turbulence of different types of ionized gas.
- To investigate distant optically-obscured HII regions.
- To determine the large-scale structure of the Galaxy as traced by ionized gas.
- To obtain the helium abundance.
- To distinguish between thermal and non-thermal sources (e.g. HII regions and supernova remnants).

1.2.1 Hydrogen and Helium Recombination Lines

Radio recombination lines of hydrogen are observed in emission from classical HII regions, planetary nebulae, diffuse ionized gas, low-density envelopes of HII regions, the partially ionized medium next to HII regions, external galaxies and a few cases of circumstellar envelopes.

Hydrogen and helium lines were first detected from hot **H II** regions ($T_e \sim 10^4 \text{ K}$) and these clouds have been extensively studied using these lines. Planetary nebulae which, like **H II** regions, are characterized by high temperatures and also high densities are also studied using hydrogen recombination lines. Hydrogen lines have been observed towards **H II** regions at wavelengths ranging from millimeters ($\nu \sim 150 \text{ GHz}$, $n \sim 40$) to meters ($\nu \sim 140 \text{ MHz}$, $n \sim 350$) (Gordon 1989, Sorochenko *et.al.* 1988, D. Hoang-Binh *et.al.* 1985, Hart & Pedlar 1976, Lockman 1976, Lockman 1980, Pedlar *et.al.* 1978, Anantharamaiah 1984, Anantharamaiah *et.al.* 1990). **RRLs** of hydrogen at different frequencies are sensitive to different physical conditions. The high-frequency ($\nu > 2 \text{ GHz}$) lines arise in hot, dense and fully ionized regions with typical line widths of $\sim 25 \text{ kms}^{-1}$ and line-to-continuum ratios of 0.01 to 0.1. At low frequencies ($\nu < 2 \text{ GHz}$) however, the effects of continuum optical depths and pressure broadening in dense ionized regions make the recombination lines from the same regions undetectable. Instead the lines at low frequencies arise in hot, tenuous parts of fully ionized regions with typical line-to-continuum ratios of a few times 10^{-3} .

Towards many **H II** regions (*e.g.* W3, **NGC2024**), in addition to the broad ($\geq 25 \text{ kms}^{-1}$) hydrogen line, a narrow hydrogen line is also detected at frequencies near 1 GHz . The width of the narrow hydrogen line rules out an origin in the hot, ionized gas but is likely to arise in the partially ionized medium (PIM) surrounding the hot gas, ionized by the photons that escape the **H II** region. Carbon lines are also observed from such partially ionized regions.

Radio recombination lines of hydrogen from positions in the galactic plane which were devoid of bright radio continuum sources were first detected by Gottesman & Gordon (1970) at 1.6 GHz and Jackson & Ker (1971) near 5 GHz . They suggested that these broad ($\sim 100 \text{ kms}^{-1}$) lines were formed in distributed ionized gas in the Galaxy. Since then, various recombination line surveys in **H166 α** by Hart & Pedlar (1976) & Lockman (1976) and in **H271 α** by Anantharamaiah (1984) have observed lines from many positions in the Galactic plane. Analysis of these data show that these lines arise in the low-density envelopes of classical **H II** regions and in large evolved low-density **H II** regions.

Many attempts to detect the WIM (McKee & Ostriker 1977) using radio recombination lines of hydrogen have been made (Shaver 1975, Shaver *et.al.* 1976, Hart & Pedlar 1980, Anantharamaiah & Bhattacharya 1986, Anantharamaiah *et.al.* 1990), but the medium has eluded detection. The absence of contribution by the WIM to the hydrogen line near 145 MHz detected towards the Galactic centre by Anantharamaiah *et.al.* (1990) implies that $T_e > 6700 \text{ K}$, $n_e < 0.2 \text{ cm}^{-3}$ and the filling factor of the

WIM is $> 60\%$.

Towards the Galactic centre (GC) hydrogen recombination lines have been observed at frequencies ranging from 23 GHz (Rodriguez & Chaisson 1979) to 145 MHz (Anantharamaiah *et.al.* 1990). The lines at higher frequencies ($\nu > 1.4$ GHz) sample the entire line-of-sight to the GC and are observed to be very broad ($AV \geq 150 \text{ kms}^{-1}$). The major contribution to the line emission at these frequencies comes from ionized gas close to the Galactic centre, with large non-circular motions. The width of the lines from the central regions are large ($AV > 150 \text{ kms}^{-1}$) (see Roelfsema & Goss 1992). At low frequencies ($\nu < 1$ GHz), only the line-of-sight gas is sampled by recombination lines (Pedlar *et.al.* 1978, Anantharamaiah & Bhattacharya 1986). Shaver (1975) showed that stimulated emission is expected to be important in transitions at frequencies below 500 MHz and this has indeed been observed towards this direction.

Interesting recombination lines at mm-wavelengths were detected from the circumstellar disk of the Be star, **MWC349** by Martin-Pintado *et.al.* (1989). The lines observed from this star due to transitions between levels with $n > 36$ follow **LTE**. However the lines detected for $n < 36$ are many times stronger than the **LTE** predictions owing to strong stimulated emission. Although almost all the recombination lines detected towards HII regions have a component of stimulated emission, the mm wave lines towards **MWC349** are true maser lines. The negative optical depths are large and the lines are narrow and time variable.

H359 α ($\nu \sim 142$ MHz) detected from the direction of the Galactic centre (Anantharamaiah *et.al.* 1990) is the lowest frequency hydrogen recombination line detected so far. Attempts to observe much lower frequency lines of hydrogen (2426 MHz; $n=650$ to 630) from several directions in the Galaxy have yielded negative results (Konvalenko & Sodin 1979, Sorochenko & Smirnov 1993) with an upper limit of 3×10^{-4} for the line-to-continuum ratio.

Hydrogen RRL have also been detected from the central regions of starburst and seyfert galaxies. **H166 α** from M82 (Shaver *et.al.* 1977) and **H102 α** in NGC 253 (Seaquist & Bell 1977) were the first recombination lines detected from external galaxies. Since then, many more external galaxies have been searched in recombination lines of hydrogen (Anantharamaiah *et.al.* 1993) and lines have been detected in several starburst galaxies (Zhao *et.al.* 1996). NGC 253 has been mapped at high resolution in hydrogen recombination lines over a range of frequencies (Anantharamaiah & Goss 1990) and remarkable kinematics have been observed from the nuclear region using recombination lines (Anantharamaiah & Goss 1996).

RRL of helium are generally detected from HII regions around massive OB stars

where ultraviolet photons with energies in excess of 24.4 eV can ionize helium. The helium recombination line is separated from the hydrogen line by 125 km s^{-1} due to the difference in the reduced mass of the two atoms. In principle, the ratio of hydrogen and helium lines can be used to derive their relative abundances which is an important parameter to constrain cosmological models. However care should be taken since the **He II** and **H II** regions may not be coextensive due to their different ionization potentials. In some cases, very anomalous **He/H** ratios have been derived from observation of radio recombination lines (Roelfsema *et.al.* 1992)

1.2.2 Radio Recombination Lines of Carbon

Soon after the first detection of a radio recombination line in 1965, Palmer *et.al.* (1967) reported the detection of a narrow 'anomalous' line at a frequency higher than that of the **H109 α** line in the directions of **NGC2024** (Orion B) and **IC1795** (W3) and identified it as the **C109 α** line. The ratio of the intensities of the carbon and hydrogen lines was found to be about two orders of magnitude larger (Goldberg & Dupree 1967) than the ratio of their cosmic abundances. The lines were also very narrow ($< 10 \text{ km s}^{-1}$). This immediately indicated that the intense carbon line must arise in a region of very different physical conditions. Further observations of carbon lines towards **H II** regions not only found the width of the carbon line to be incompatible with an origin in the **H II** region itself, but even the radial velocity was found to be different, again suggesting a different site of origin. Furthermore, the carbon lines showed a different dependence on frequency.

Most of the stellar radiation of wavelength **longward** of 91.2 nm escapes from **H II** regions and can ionize heavier elements with ionization potential less than 13.6 eV in the surrounding neutral medium. Carbon, whose first ionization potential is 11.4 eV and which is the fourth most abundant element in the ISM is likely to be singly ionized in this medium. Some photons shortward of $\lambda = 91.2 \text{ nm}$ **also** escape from the **H II** region and may also succeed in ionizing a small fraction of the neutral hydrogen in the surrounding medium which is known as the partially ionized medium (PIM). The fractional ionization of hydrogen is much less in the PIM than that in **H II** regions. Beyond the PIM is the photodissociation region (PDR), the extent of which is generally measured in terms of extinction in the visible band (Tielens & Hollenbach 1985). The region is defined by these authors as "regions where FUV radiation (6 – 13.6 eV) dominates the heating and/or some important aspect of the chemistry." In fact PDR is sometimes taken to represent Photon Dominated Regions. The PDR contains both atomic and molecular hydrogen regions. A schematic showing the structure of a PDR in

relation to a HII region is displayed in Fig 1.2 which is taken from Tielens & Hollenbach (1985). Narrow carbon lines observed at high frequencies probably originate in the PIM

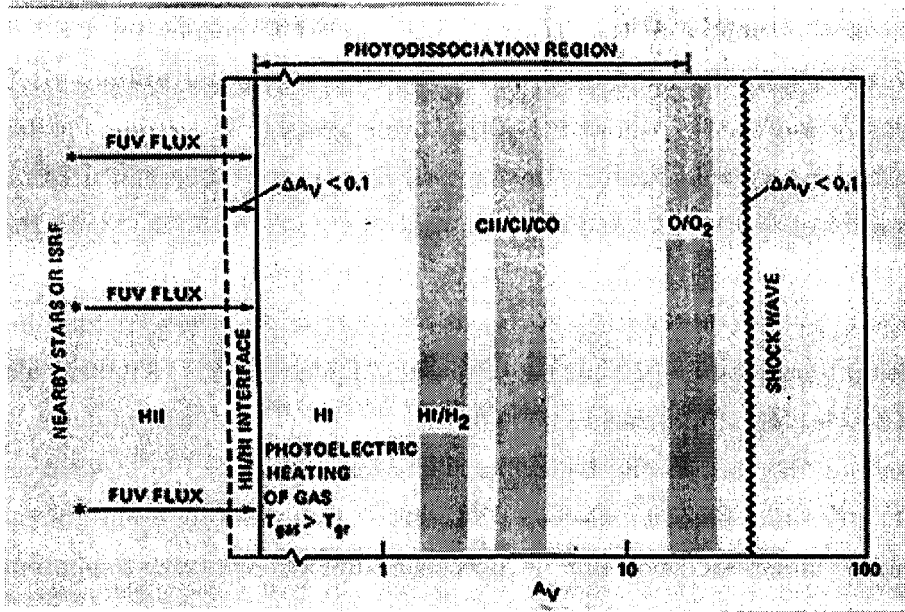


Figure 1.2 Schematic of a photodissociation region (PDR) taken from Hollenbach (1990)

or PDR associated with HII regions. The typical temperatures at the site of origin are believed to be a few hundred Kelvins and the typical electron densities are a few tens per cm^3 (Pankonin *et.al.* 1977). Such electron densities imply atomic hydrogen densities of $> 10^5 \text{ cm}^{-3}$. PIMs associated with many HII regions like W3 and NGC2024 have been observed in narrow carbon and narrow hydrogen lines. The difference in radial velocities of broad hydrogen lines and narrow carbon & hydrogen lines is observed to be non-zero in addition to the widely different widths thus providing evidence to their origin in distinct regions. Moreover, the narrow hydrogen and carbon lines also show a slight difference in their central velocities (Pankonin *et.al.* 1977). Both, the narrow hydrogen and carbon lines at lower frequency ($\sim 1 \text{ GHz}$) are intensified by stimulated emission of the strong continuum emission from the HII regions (Pankonin *et.al.* 1977, Onello & Phillips 1995). Towards the end of this thesis, we present an observational study of the HII region W3 which has associated PIM & PDR.

A completely different type of carbon recombination line was discovered by Konovalenko & Sodin in 1980. Using the low-frequency (12-26 MHz) large radio telescope at Ukraine, Konovalenko & Sodin (1980) detected an absorption feature near 26.13 MHz towards the strong non-thermal radio source Cas A. Although the line was initially thought to be due to interstellar nitrogen, it was correctly identified by Blake,

Crutcher & Watson (1980, hereafter **BCW80**) as a recombination line of carbon due to transition between $n = 631$ to $n = 632$. The identification was confirmed when **C630 α** was also detected (Konovalenko & **Sodin** 1981) from the same direction. These recombination lines were unique in that they were the lowest frequency lines yet detected and furthermore they were the first lines to be detected in absorption. **BCW80** & Konovalenko & **Sodin** (1981) showed that the regions giving rise to these low-frequency lines could be cold regions along the line of sight with electron temperature of ~ 50 K, electron density of $\sim 0.1 \text{ cm}^{-3}$ and emission measure of $\sim 0.07 \text{ pc cm}^{-6}$. In these cold regions, carbon could be ionized by the background ultraviolet radiation.

Since then the direction towards Cas A has been extensively investigated in carbon recombination lines ranging in frequency from 14.7 MHz ($n=768$) (Konovalenko 1990) to 1451 MHz ($n=165$) (Sorochenko & Walmsley 1991). These low frequency lines of carbon show another interesting behaviour. The lines which are in absorption below ~ 100 MHz, turn into emission above ~ 200 MHz. This turnover from absorption to emission can be understood from simple physical arguments regarding the population of various quantum number states. At some quantum numbers, inversion of populations results from the dominance of radiative processes in redistributing the electrons between various levels. This results in stimulated emission lines. However for higher quantum numbers, the larger size of the excited atoms leads to increased collisions in the plasma which establish normal populations. For these thermalized levels, since $T_{ex} \sim T_e$ and $T_e \ll T_{bg}$, the atoms absorb the background radiation resulting in absorption lines. Although the turnover from emission lines to absorption lines with increasing n is theoretically expected, the exact n at which it occurs depends on the detailed physical properties of the medium. Another effect which is important at low frequencies is line broadening due to electronic collisions and strong non-thermal radiation field which are strong functions of n .

Two types of models have been considered to explain the carbon recombination lines observed towards Cas A. In the cold gas model, the carbon lines are believed to arise in clouds with $T_e \sim 20$ K and $n_e \sim 0.3 \text{ cm}^{-3}$ and the ionized carbon could be associated with molecular clouds (Ershov *et.al.* 1984, 1987). In the warm gas model, the carbon lines arise in clouds with $T_e = 35\text{-}100$ K and $n_e = 0.05\text{-}0.15 \text{ cm}^{-3}$ (Konovalenko & **Sodin** 1981, Konovalenko 1984, Golyntin & Konovalenko 1990, Payne, **Anantharamaiah**, & Erickson 1989, hereafter **PAE89**, Payne, **Anantharamaiah**, & Erickson 1994, hereafter **PAE94**) and these regions could be identified with neutral HI clouds in the Galaxy. In the warm gas model a dielectronic-like recombination process first suggested by **WWC80** plays a significant role in determining the level populations of high quan-

tum states of carbon. This process involves the fine structure states $^2P_{3/2}$ & $^2P_{1/2}$ with a energy separation of ~ 92 K in singly-ionized carbon. In this process, an energetic electron can recombine to a high- n state after losing its extra energy to the fine-structure excitation of a core electron. Owing to this process, level populations at certain n become suprathermal, hence enhancing the line optical depths. At low temperatures, as expected, the effect of this process decreases. As recombination data towards Cas A at more frequencies has become available, the cold gas models have not been able to explain the observed variation in optical depth with frequency and evidence supporting the warm gas models seem to be increasing.

Low-frequency carbon recombination lines of the kind observed towards Cas A have been detected from several other directions in the Galaxy. Around 25 MHz, lines have been detected towards the dust cloud L1407 (Golyntkin & Konovalenko 1990), towards the Galactic plane position G75+00 (Konovalenko 1984, Anantharamaiah *et al.* 1988) and the H II regions NGC2024, DR21 and 5140 (Konovalenko 1984, Golyntkin & Konovalenko 1990). Towards the H II region M16, carbon recombination lines have been detected in absorption at 69 & 80 MHz and in emission at 328 MHz (Anantharamaiah *et al.* 1988). Around 76 MHz, carbon recombination lines have been detected in absorption from many positions in the Galactic plane in the longitude range of 340° to 20° (Erickson *et al.* 1995). Although, the above observations (except that of Erickson *et al.* 1995) have been made in the direction of specific sources, it appears that the low-frequency lines themselves do not arise in these sources but somewhere along the line of sight.

Towards the Galactic centre, carbon recombination lines have been detected at a number of frequencies below 1 GHz (Pedlar *et al.* 1978, Anantharamaiah 1984, Roshi & Anantharamaiah 1997). These lines also fall in the same category as the lines observed towards Cas A. The observed lines are in absorption below 100 MHz and in emission above 200 MHz. The site of origin of these lines also appears to be the cold neutral gas along the line of sight towards the Galactic centre (Roshi & Anantharamaiah 1997).

In summary, carbon recombination lines have been observed over a wide range of frequencies from many directions in the Galaxy and these lines have become effective diagnostic tools of the partially ionized gas in the ISM. Carbon RRLs seem to arise in two distinct kinds of regions. Higher frequency lines ($\nu > 1$ GHz) arise in partially ionized zones adjacent to hot, dense H II regions. The lower frequency ($\nu < 1$ GHz) lines seem to arise in a wide spread component, possibly the CNM of the ISM. The region which gives rise to the carbon RRLs may also contribute to the [CII]158 μ m line emission observed in the galactic plane. While the properties of the region giving rise

to the higher frequency carbon RRLs seem to be reasonably well understood, the properties of the low-frequency carbon lines and their association with other components of the ISM is poorly known. The purpose of this thesis is to make an observational study of the regions in the galactic plane which produce the low-frequency carbon **m**-combination lines. In addition, a specific PIM around the **H II** region W3 is studied in carbon and hydrogen RRLs at a relatively high frequency *i.e.* 1.4 **GHz**.

1.3 Preview of the Present Work

Most of the work presented in this thesis is related to the observations of that class of **C II** regions which are seen by low-frequency ($\nu < 500$ MHz) carbon recombination lines. We have searched for carbon recombination lines in the **Galactic** plane near 34.5 **MHz** using the low-frequency '**T**'-shaped dipole array at Gauribidanur and near 328 MHz using the Ooty radio telescope, Using these telescopes, we have **also** made observations in the direction towards **Cas A**. Complementary observations were obtained near 330 MHz using the Very Large Array in the USA towards one position in the Galactic plane and also towards Cas A. **Furthermore**, for comparison with the carbon line-forming regions, we obtained the distribution of molecular gas, in front of Cas A by mapping the ^{12}CO line using the 10.4m telescope at RRI, **Bangalore**. Finally, we have also obtained observations, using the VLA, of carbon and hydrogen **RRLs** near 1.4 **GHz** towards the **H II** region, W3. In this thesis, we present the instruments, the observing techniques, the data analysis, the results and interpretation of all the above observations. This thesis is organized as follows:

In Chapter 2, some physical theory of recombination lines is presented.. **Radiative** transfer for the line intensity as it journeys to the radio telescope encountering matter and radiation on its way is briefly explained. The various line broadening mechanisms, the calculation of departure coefficients quantifying non-LTE level populations, the **effect** of **dielectronic-like** capture on level populations of carbon, the interpretation of radio recombination **line** observations and the dependence of line formation on frequency are also discussed in this chapter.

In Chapter 3, the instruments used, the observing technique followed, data analysis and results of the observations are detailed. We detected carbon **RRLs** in absorption at 34.5 MHz from 10 positions out of the total 35 positions that were observed using the Gauribidanur array. This included the detection of a Voigt-shaped profile from the direction of **Cas A**. Most of the above positions were also observed in emission lines at 328 MHz using the Ooty Radio Telescope. Since the angular resolution of single-

aperture telescopes at low frequencies is poor, one of the Galactic plane positions, G14+00 was observed with an aperture synthesis telescope, VLA at 330 MHz resulting in high angular resolution. However, no carbon line emission was detected. To study the association of carbon line-forming gas with other components of the ISM, ^{12}CO emission (~ 115 GHz) was mapped across Cas A. The different sections of Chapter 3 are devoted separately to each of the above observations. Within these Sections, the scientific aim for observing at a certain frequency, the telescope used, the observing technique and the results are presented.

In Chapter 4, the results of carbon recombination line observations towards Cas A are discussed. The models which fit the data and association with other components of the ISM are presented. Our observations support the scenario of association of the partially ionized gas with the cold neutral medium of the ISM. Limits on the physical parameters of the medium are derived from the pressure & radiation broadened Voigt profile at **34.5 MHz**.

Chapter 5 presents the models which fit the absorption and emission lines of carbon observed from the inner Galactic plane. Results of both, low-temperature models which are typical of conditions in molecular clouds and relatively high-temperature models which are typical of CNM in the ISM are examined. Dielectronic-like recombination influences the level populations in both the cases. The results of these models, importance of the cloud size in determining the models and the association of this partially-ionized gas with other components of the ISM are discussed.

In Chapter 6, VLA observation of carbon and hydrogen recombination lines near 20 cm from the HII region complex W3 is presented. Broad ($> 25 \text{ km s}^{-1}$) and narrow ($< 10 \text{ km s}^{-1}$) components are detected in the hydrogen line. The distributions of carbon and hydrogen line intensities across the continuum source are compared. While the broad line region resembles the continuum morphology the narrow lines trace different distributions. The physical parameters of the emitting region, the PIM, are obtained by model fits to the observed line emission.

The results of the work described in the thesis are summarized in Chapter 7. Future work which may further our understanding of the CII regions is also suggested.

Chapter 2

Some theory of Radio Recombination Lines

2.1 Introduction

When an external radiation field consisting of photons of sufficient energy illuminates a neutral medium, it sets in motion the process of ionization of the constituent elements, and the reverse process of recombination follows. Ionization equilibrium is established when the rate of ionization is balanced by the rate of recombination, as for example, in HII regions in the Galaxy. In these clouds, it is the **stellar** radiation that maintains the ionization. Recombination lines are emitted from an ionized nebula when a free electron is captured in an excited atomic state from which it then radiatively cascades down to the ground state. The relative populations of the atomic levels participating in a given transition can be conveniently described in terms of an 'excitation temperature', T_{ex} which is defined by the **Maxwell-Boltzmann** formula, $\frac{n_2}{n_1} = \frac{g_2}{g_1} \exp(-\frac{E_2 - E_1}{kT_{ex}})$. Here n_1 and n_2 are the actual occupation numbers of levels 1, 2 which have statistical weights of g_1 and g_2 . Under non-equilibrium conditions, which often prevail in certain regions of the ISM, this excitation temperature **is** a function of the quantum number. The level populations are said to be in thermal equilibrium with the free plasma when the excitation temperature approaches the 'kinetic temperature' which is defined by the **Maxwellian** velocity distribution of the electrons and ions **within** the cloud. Thermal equilibrium is expected at large quantum numbers where the level populations are essentially determined by collisions. The electron cascade produces photons with energies ranging from that of long radio waves (e.g. principal quantum number $n \sim 550$) to the ultraviolet (Lyman lines, principal quantum number $n \sim 1$). The recombination lines span a wide range of the electromagnetic spectrum. The strengths **and** widths of recombination lines are sensitive functions of the conditions existing at their origin.

Recombination lines are therefore used as diagnostics of ionized media.

The line formation at different frequencies which correspond to transitions between different quantum numbers, is controlled by different physical processes. Recombination lines at high frequencies are sensitive to high-density regions whereas those at low frequencies trace low-density, cooler regions of the Galaxy. Hence recombination lines over a range of frequencies can be used to probe physical conditions existing in different ionized media. At small- n , radiative processes control the level populations and move them towards non-equilibrium values. At these values of n , inverted populations (negative excitation temperature) result from the relatively faster cascade to lower levels from some level n as compared to the cascade from higher levels to that level. This is because the Einstein coefficient, $A_{n, n-1}$ for spontaneous emission is a strong function of n ; $A_{n, n-1} \propto \frac{1}{n^3}$. The phenomenon of inverted populations gives rise to maser emission when a continuum background is present. On the otherhand, at large- n , atoms are larger, collisions are felt more frequently which thermalize these states. The level populations and therefore the line strengths are thus determined by various physical processes. Departures from local thermodynamic equilibrium (LTE) are central to understanding the line emission produced under a range of conditions and these have to be understood and quantified in order to use radio recombination lines (RRL) as probes of the conditions in the ISM.

The line radiation emitted by an atom is modified by encounters with other particles or radiation in the intervening medium as it traverses the line of sight towards us. The theory of radiative transfer describes this phenomenon. In this chapter, we discuss the equation of radiative transfer and the physics of line formation with emphasis on low-frequency RRL which arise from transitions between large quantum numbers.

2.2 Recombination Line Frequencies

The frequency ν , of a transition from an upper level of principal quantum number m to a lower level n is given by the Rydberg formula:

$$\nu = R_{\infty} c Z^2 \left(\frac{1}{n^2} - \frac{1}{m^2} \right) \quad (2.1)$$

where

- ν = the rest frequency of the emitted photon
- m = principal quantum number at which the transition begins.
- n = principal quantum number at which the transition ends.
- c = the velocity of light = $2.99272 \times 10^8 \text{ m s}^{-1}$

Z = effective nuclear charge of the recombining ion.

$R_a = 1097.3731 \left(1 + \frac{m_e}{M_a}\right) m^{-1}$ is the Rydberg constant for an element a.

M_a = atomic mass.

m_e = electronic mass = 9.11×10^{-31} kg.

For most practical purposes where $\Delta n = m - n \ll n$ (radio frequencies), Eqn 2.1 can be approximated by

$$\nu = \frac{2R_a c Z^2 \Delta n}{n^3} \quad (2.2)$$

The difference between the frequencies of transitions between two consecutive pair of levels is then approximated by:

$$\Delta\nu = \frac{2R_a c Z^2}{n^4}. \quad (2.3)$$

Nomenclature : For a transition in the Carbon (C) atom, if $m = n + 1$, then the line is denoted by $Cn\alpha$, if $m = n + 2$ then $Cn\beta$ and likewise if $m = n + 3$, $n + 4$, ... then $Cn\gamma$, $Cn\delta$ For transitions at different n , the size of the atom is given by

$$r = a_0 n^2 Z^{-1} \text{ nm} \quad (2.4)$$

where

a_0 = the Bohr radius = 0.05 nm

Thus for a transition **from** $m = 2$ to $n = 1$, the radius of a carbon atom is of the order of the Bohr radius whereas for a transition from $m = 574$ to $n = 575$, the radius of the carbon atom is $16.5 \mu\text{m}$ - more than 10^5 times the Bohr radius ($Z = 1$ for a carbon atom with outermost electron in $n=575$ orbit). The Rydberg atom in interstellar space has assumed large linear dimensions which are practically unrealizable under terrestrial densities. Such atoms are likely to be collisionally ionized in the terrestrial atmosphere before they can radiatively **de-excite**.

2.3 The Radiative Transfer Equation

Radiation emerging from a nebula carries information about the physical properties of the medium. As the radiation travels through space (within and outside the nebula), it interacts with matter which modifies its nature. Hence the radiation that arrives at the radio telescope bears the imprint both of the original radiation process (which we want

.to know about) and of **the propagation** (whose effects we need to **remove**). The theory of radiative transfer must be applied to understand the physical conditions at the origin from the observed intensity. **The theory encompasses** possibilities like a background radiation field that gets modified while propagating through the nebula, radiation from the nebula that gets amplified or attenuated during its passage through the nebula and a foreground radiation field that adds to the radiation emerging from the nebula. In this section, **we** discuss the radiative transfer equation with **approximations** appropriate for radio wavelengths, if required. We start with a short discussion of the emission and absorption coefficients.

Consider a beam of radiation traversing a cloud of **gas**. During the passage through the cloud, the intensity of the beam can get amplified or **attenuated** depending on the physical conditions in the **gas**. The emission and absorption coefficients are the quantifying parameters for this process. The energy emitted by the gas per unit time per unit solid **angle** and per unit **volume** is given by the emission coefficient. The total emission coefficient at the centre of a RRL at frequency ν is

$$j_{\nu} = j_c + j_l. \quad (2.5)$$

where

$$\begin{aligned} j_{\nu} &= \text{total emission coefficient at } \nu, \text{ Watts } \text{m}^{-3} \text{ ster}^{-1} \text{ Hz}^{-1} \\ j_l &= \text{line emission coefficient at } \nu, \text{ joule } \text{m}^{-3} \text{ s}^{-1} \text{ ster}^{-1} \text{ Hz}^{-1} \\ j_c &= \text{continuum emission coefficient at } \nu, \text{ joule } \text{m}^{-3} \text{ s}^{-1} \text{ ster}^{-1} \text{ Hz}^{-1} \end{aligned}$$

The decrease in the beam intensity per unit length is characterized by the absorption coefficient. **From Kirchoff's** law, the ratio of the emission coefficient to the absorption coefficient in **LTE** is the Planck function, $B_{\nu}(T_e)$. Hence

$$j_{\nu} = B_{\nu}(T_e)(\kappa_c + b_n \kappa_l^{*1}) \quad (2.6)$$

where

$$\begin{aligned} \kappa_c &= \text{continuum absorption coefficient, } \text{m}^{-1} \\ \kappa_l^{*} &= \text{LTE line absorption coefficient, } \text{m}^{-1} \\ B_{\nu}(T_e) &= \text{Planck function, joule } \text{m}^{-2} \text{ s}^{-1} \text{ ster}^{-1} \text{ Hz}^{-1} \end{aligned}$$

¹A superscript ^{1*} on any parameter indicates its **LTE** value.

b_n is the departure coefficient, first introduced by Menzel (1937). It is defined as the ratio of the non-LTE level populations, N_n , to the equilibrium level populations, N_n^* . N_n^* is given by Saha equation:

$$N_n^* = N_e N_i \left[\frac{h^2}{2\pi m_e k T_e} \right]^{1.5} \frac{g_n}{2} e^{\chi_n} \quad (2.7)$$

where

N_i = Ionic density, cm^{-3}

N_e = electron density, cm^{-3}

g_n = statistical weight for level n, dimensionless

$$\chi_n = \frac{h R_a c Z^2}{n^2 k T_e} \quad (2.8)$$

Under conditions which are typical in ionized gas in the ISM, various physical processes act to move the level populations away from equilibrium values. The departure coefficient measures this deviation and it is necessary to understand its behaviour for modelling the observed RRL intensities.

The total absorption coefficient at the centre of a spectral line is

$$\kappa_\nu = \kappa_c + \kappa_l = \kappa_c + b_n \beta_n \kappa_l^* \quad (2.9)$$

where

$$\beta_n = 1 - \frac{k T_e}{h \nu} \frac{d(\ln b_n)}{dn} \quad (2.10)$$

is the correction factor to the LTE line-absorption coefficient for stimulated emission (Goldberg 1966). At radio frequencies, $k T_e / h \nu \gg 1$ for probable values of T_e and for increasing b_n with n, the differential term is positive which results in a negative value of β_n . As the line absorption coefficient is $\kappa_l = b_n \beta_n \kappa_l^*$, a negative value of β_n implies negative absorption or in other words, stimulated emission. Stimulated emission makes a significant contribution to the line strength and begins to dominate the line emission at low frequencies.

Consider again a beam travelling from a celestial source to the telescope. Let I be the intensity (defined as the energy crossing an area dA in time dt in a frequency range $d\nu$ within a solid angle $d\Omega$) of the beam incident on the telescope. The change in the intensity of the beam due to emission and absorption in the intervening medium before it reaches the telescope is

$$\frac{dI_\nu}{dt} = j_\nu - \kappa_\nu I_\nu \quad (2.11)$$

where dl is the distance travelled by the **beam** along the line of sight. The absorption coefficient κ_ν consists of contributions from **both** the 'true' absorption **and** stimulated emission (negative absorption), both of **which** depend on the intensity of the incoming beam. Hence the net absorption **can** be **positive** or negative, depending **on** which of the two processes dominate in Eqn 2.9.

Eqn 2.11 is the radiative transfer equation. **One can** solve for the intensity of the emerging beam if one knows the emission and absorption **coefficients** of the intervening medium. These depend on the physical processes operating in that medium. Hence, most of the modelling is aimed at understanding and quantifying these processes for the system under study.

The radiative transfer equation is generally expressed in terms of the optical depth measured along the path of **a ray**. The differential optical depth is defined **as**:

$$d\tau_\nu = \kappa_\nu dl \quad (2.12)$$

For a homogeneous medium of length L , the optical depth is given by,

$$\tau_\nu = \kappa_\nu L \quad (2.13)$$

Optical depth is a function of frequency and it is a useful measure of the penetration depth into the medium for photons of various energies. A medium is called optically thick at some frequency ν if $\tau_\nu > 1$. If $\tau_\nu < 1$, then the medium is called optically thin.

Division of the radiative transfer equation **Eqn 2.11** by κ_ν gives the equation in terms of the optical depth. The absorption and emission over the extent of the medium are directly measured by this form of the equation:

$$\frac{dI_\nu}{d\tau_\nu} = -I_\nu + S_\nu \quad (2.14)$$

where S_ν is the source function of the medium which approaches the Planck's function $B_\nu(T_e)$ in LTE. In this equation, the contribution from the non-thermal radiation field within and in front of the cloud have been neglected. The optical depth at the line center is $\tau_\nu = \tau_L + \tau_C$ where τ_L and τ_C are the line and continuum optical depths respectively.

It is not trivial to solve **Eqn 2.14** to get the emerging intensity for a **realistic** distribution which has variations in electron temperature and density over different spatial scales within the medium. **However**, it is useful to consider a simple model with a homogeneous, isothermal distribution of **gas**, in order to get a handle on the average physical conditions in the cloud. Using the Rayleigh-Jeans approximation to the **Planck's** radiation law which is valid at long radio wavelengths, the intensity in Eqn 2.14 can be

replaced by the brightness temperature, $I = \frac{2kT_B}{\lambda^2}$. With the above assumption of a homogeneous, isothermal mass of gas, solution of Eqn 2.14 for the continuum brightness temperature (Shaver 1975) is

$$T_C = T_o e^{-\tau_C} + T_e (1 - e^{-\tau_C}) \quad , \quad (2.15)$$

and for the brightness temperature at the line frequency is

$$T_L + T_C = T_o e^{-\tau_\nu} + T_e \left[\frac{(b_m \tau_L^* + \tau_C)}{\tau_\nu} (1 - e^{-\tau_\nu}) \right] \quad . \quad (2.16)$$

Hence the net line intensity at the line frequency in terms of brightness temperature is given by

$$T_L = T_o [e^{-\tau_C} (e^{-\tau_L} - 1)] + T_e \left[\frac{(b_m \tau_L^* + \tau_C)}{\tau_\nu} (1 - e^{-\tau_\nu}) - (1 - e^{-\tau_C}) \right] \quad (2.17)$$

where T_o is the equivalent brightness temperature of the background radiation field.

For a **homogeneous**, isothermal medium where the continuum emission at radio frequencies is due to **bremsstrahlung** (free-free emission), the continuum optical depth is given by (from Oster 1961)

$$\tau_C = 3.14 \times 10^{-2} \frac{EM_c}{T_e^{1.5\nu^2}} \left[1.5 \ln \left(\frac{T_e}{K} \right) - \ln \left(\frac{20.18\nu}{GHz} \right) \right] \quad (2.18)$$

where $EM_c = \int N_e^2 dl$ pc cm^{-6} is the continuum emission measure. The LTE line optical depth is given by (from Shaver 1975)

$$\tau_L^* = 1.92 \times 10^3 \frac{EM}{(\frac{\Delta V_D \nu}{c}) T_e^{2.5}} Z^2 e^{X_n} \left[1 + 1.48 \frac{\Delta V_L}{\Delta V_D} \right]^{-1} \quad (2.19)$$

where $EM = \int N_e N_i dl$ is the line emission measure of the recombining ion in pc cm^{-6} . The line optical depth which includes corrections due to non-LTE effects is given by

$$\tau_L = b_n \beta_n \tau_L^* \quad (2.20)$$

The integral of the line optical depth over the line width is given by

$$\int \tau_L d\nu = 2.046 \times 10^6 T_e^{-5/2} \exp \left(\frac{1.58 \times 10^5}{n^2 T_e} \right) EM_i b_n \beta_n \quad s^{-1} \quad (2.21)$$

However, it is not possible to use Eqn 2.17 to directly obtain electron density or electron temperature from the measured line strength. One has to use iterative procedures which generally involve some initial guesses of the physical conditions in the cloud in addition to measurements of line intensities at a number of frequencies. When using the iterative procedure, the expected line intensities are calculated from Eqn 2.17

or the integrated optical **depths** from Eqn 2.21 and **compared** with the observed values. What makes the **determination** of the physical properties of the **emitting medium** difficult is the dependence of the departure coefficients, optical depth and the observed line strengths on the electron temperatures and densities and the dependence of the latter on the former. A direct solution for T_e^* can only be obtained under condition of LTE in optically thin ($\tau_L \ll \tau_C \ll 1$) nebula.

2.4 Recombination Line Profiles

A recombination line (RL) is emitted by an atom when a bound electron jumps between **two** quantum **levels**; the energy difference between the two levels appearing as a spectral line. The energy of the spectral line is not confined to a single frequency but spread **over** a range of frequencies determined by many broadening mechanisms. In addition to natural broadening, which **arises** due to the finite lifetime of the quantum level, other mechanisms, described below, act to broaden the line further. The resulting spectral line can be described by a profile function $\phi(\nu)$ that is determined by various physical processes in the nebula. The profile function links the width and centroid of emission to physical parameters like temperature, **turbulence** and density in the cloud. The profile functions are normalized so that the area under the profile is unity *i.e.* $\int \phi(\nu) d\nu = 1$. The following profile functions are relevant for **RRLs**.

Gaussian Profile Function

Doppler **broadening**:

Velocities of particles in thermal equilibrium follow the **Maxwellian** distribution. The distribution of velocities of the particles emitting at a certain frequency results in a distribution of frequencies when seen in the observer's frame due to the Doppler effect. The resulting spectral distribution is a Gaussian which can be written in terms of ΔV_D , the full width at half maximum (FWHM), in units of velocity as follows (from Shaver 1975):

$$\phi_D(V) = \frac{2\sqrt{\ln 2}}{\sqrt{\pi}\Delta V_D} \exp \left[- \left(\frac{2\sqrt{\ln 2}(V - V_0)}{\Delta V_D} \right)^2 \right]. \quad (2.22)$$

Doppler effect due to the thermal and turbulent motions in the plasma produces a Gaussian line profile. The width of the spectral line is given by (from Shaver 1975)

$$\Delta V_D = 2\sqrt{\ln 2} \left[\frac{2kT_e}{M_i} + \frac{2}{3} \langle V_t^2 \rangle \right]^{1/2} = 2\sqrt{\ln 2} \left[\frac{2kT_D}{M_i} \right]^{1/2} \quad (2.23)$$

where

$\langle V_t^2 \rangle$ is the mean square of the distribution of turbulent velocities.

T_D is the Doppler temperature.

M_i is the mass of the emitting ion.

k is the **Boltzmann's** constant $1.38 \times 10^{-23} \text{ JouleK}^{-1}$

The Doppler temperature includes contributions **from** both thermal and turbulent motions in the plasma. In most of the spectral lines arising in the cold regions of the ISM, the line width is dominated by turbulence. It is difficult to obtain an estimate of turbulence and hence from Eqn 2.23, only an upper limit on the kinetic temperature for the plasma can be derived **from** the thermal line width. If RRL from two species with different masses, arising in the same cloud can be observed, then the kinetic temperature of the cloud can be determined by eliminating the effect of turbulence. With increasing plasma temperatures and turbulence, the Doppler width increases and the peak line intensity decreases, keeping the integrated line strength constant.

Lorentzian Profile Function

Natural, pressure and radiation broadenings result in a **Lorentzian-shaped** profile for the **RRL**. Natural broadening is a result of the finite lifetime of the energy levels. Pressure and radiation broadening are strong functions of the principal quantum number and hence are important for Rydberg atoms. Pressure broadening is sensitive to the electron density in the cloud and radiation broadening is sensitive to the incident radiation field.

Pressure broadening:

Collisions in the plasma (impact effect) or the effect of quasi-static electric field (Stark effect) on the emitting atoms result in this broadening. Under the conditions prevailing in the ISM, electron impacts with the emitting atom **is** the major contributor to this broadening (Griem 1967). Under the impact approximation, **if** an atom undergoes a collision with **an** electron in the plasma while it is emitting a spectral line, the phase of the emitted wave will be suddenly modified. In a **sea** of colliding and radiating atoms, this process leads to broadening of the emitted line and the resulting profile shape is a Lorentzian (from Griem 1967, Peach 1972):

$$\phi_L(\nu) = \frac{\gamma}{\pi} \frac{1}{[(\nu' - \nu)^2 + \gamma^2]} \quad (2.24)$$

where $\gamma = \Delta\nu_L/2$ is the damping constant (total rate of collision-induced decay of an atomic state) and $\Delta\nu_L$ is the Lorentzian width.

The FWHM of the profile due to pressure broadening at the high temperatures characteristic of HII regions ($T_e = 10^4$ K) (Griem 1967, Brocklehurst & Leeman 1971) is given by

$$\Delta V_P = 3.74 \times 10^{-11} \frac{N_e n^{4.4}}{T_e^{0.1}} \frac{c/(kms^{-1})}{\nu/(kHz)} kms^{-1} \quad (2.25)$$

and the ratio of pressure to Doppler broadening is

$$\frac{\Delta V_P}{\Delta V_D} = 7.98 \times 10^{-18} \frac{N_e}{T_e^{0.1}} \frac{n^{7.4}}{T_D^{0.5} \Delta n} \quad (2.26)$$

where

ΔV_P = FWHM of profile due to pressure broadening

ΔV_D = FWHM of profile due to Doppler broadening

T_D = Doppler temperature

At low temperatures the above two equations assume the following forms (Shaver 1975):

$$\Delta V_P = 2 \times 10^{-8} \exp\left(-\frac{26}{T_e^{1/3}}\right) \frac{N_e n^{5.2}}{T_e^{1.5}} \frac{c/(kms^{-1})}{\nu/(kHz)} kms^{-1} \quad (2.27)$$

$$\frac{\Delta V_P}{\Delta V_D} = 4 \times 10^{-15} \exp\left(-\frac{26}{T_e^{1/3}}\right) \frac{N_e}{T_e^{1.5}} \frac{n^{8.2}}{T_D^{0.5} \Delta n} \quad (2.28)$$

Notice that pressure broadening is proportional to approximately the fifth power of the principal quantum number. Classically, such a strong dependence happens because the radius of the atom increases as n^2 which enhances the collision crosssection (n^4). Transitions between large- n levels can be observed from low-temperature, low-density plasma before pressure broadening reduces the peak line strengths to undetectable levels. In an ionized nebula having a temperature of **50 K** and electron density of **0.1 cm^{-3}** , pressure broadening at $n=575$ is expected to be only **8.6 kms^{-1}** . These physical conditions are considered to be typical of the partially-ionized cloud from which low-frequency carbon lines are observed. On the otherhand, for conditions typical of HII regions, $T_e = 10^4$ K, $n_e = 100$ cm^{-3} , the pressure broadening for $n = 575$ is ~ 18000 kms^{-1} whereas for $n = 100$, it is expected to be ~ 8 kms^{-1} . The separation in velocity units between consecutive α ($\Delta n = 1$) lines in carbon at $n = 575$ is ~ 1500 kms^{-1} . Hence while the recombination lines from the low-density plasma will be observable, the lines from the high-density plasma would have merged with each other. The lines from transitions between quantum numbers near $n = 100$ would still be observable. The electron density derived from a pressure-broadened line is indicative of the true

electron density at the origin.

Radiation *broadening*:

An external radiation field incident on a plasma can enhance the downward transitions out of an atomic level by stimulated emission. This process can thus increase or even dominate the decay rate of a level *i.e.* the damping constant γ . Through this process, the lifetime of a level is reduced, the line width is increased and the resulting profile is a Lorentzian. An example is the Galactic non-thermal background radiation which can broaden low frequency (high-n) lines which are observed from low temperature, low-density plasma. The FWHM due to a non-thermal background radiation field is (Shaver 1975),

$$\Delta V_R = 8 \times 10^{-20} W_\nu T_{R,100} n^{5.8} \frac{c/(kms^{-1})}{\nu/(kHz)} \text{ kms}^{-1} \quad (2.29)$$

where $T_{R,100}$ is the radiation temperature of the background at 100 MHz and $\alpha = 2.6$ is the spectral index of the radiation field. α is defined such that $T_{R,100} \propto \nu^{-\alpha}$.

Voigt Profile Function:

If the physical conditions in the emitting plasma are such that both Doppler and Lorentzian **broadenings** are significant for an RRL at some frequency ν , then the shape of the resultant profile will be a Voigt function. A Voigt profile results from the convolution of the Gaussian profile **with** a Lorentzian profile. A Voigt profile function is defined as

$$\phi_\nu(\nu) = \frac{2\sqrt{\ln 2}}{\sqrt{\pi}\Delta V_D} H(a, u) \quad (2.30)$$

where

$$H(a, u) = \frac{a}{\pi} \int_{-\infty}^{+\infty} \frac{e^{-y^2} dy}{a^2 + (u - y)^2} \quad (2.31)$$

is the Voigt function, $a = 2\sqrt{\ln 2}\gamma/\Delta V_D$ and $u = 2\sqrt{\ln 2}(V' - V)/\Delta V_D$. For **small** values of a , the line centre is dominated by the Gaussian whereas the **wings are** dominated by the Lorentzian. We can **approximate the Voigt profile function** in terms of the Doppler and Lorentzian functions as follows (Shaver 1975),

$$\frac{1}{\phi_V(\nu)} = \frac{1}{\phi_D(\nu)} + \frac{1}{\phi_L(\nu)} \quad (2.32)$$

The FWHM of a Voigt can be calculated from the constituent Lorentzian and Gaussian widths as follows:

$$\Delta V_V = \frac{\Delta V_L}{2} + \sqrt{\left(\frac{\Delta V_L}{2}\right)^2 + \Delta V_D^2} \quad (2.33)$$

where $\Delta V_L = \Delta V_P + \Delta V_R$

The weak **Lorentzian** wings of the Voigt profile make their detection rather difficult. In general, long integrations and flat **instrumental** spectral response (**baseline**) are required for the detection of these wing. In Chapter 3 of this thesis, we present an observation in which a clear Voigt profile is obtained.

2.5 Calculation of Departure Coefficients

Departures of level populations from thermodynamic equilibrium can **lead** to inverted populations over a range of quantum numbers, especially those corresponding to radio frequencies. This inversion, in turn, leads to amplification of the radio **recombination** lines by stimulated emission (Goldberg 1966). The departure from equilibrium is a function of electron density and temperature in the medium. It is important to account for the non-LTE processes that influence the level populations when interpreting observed **RRL**. Departure **coefficients**, b_n and β_n describe the non-LTE effects. The ratio of the number of atoms in a certain level, n under actual conditions to the number under LTE conditions is defined as the departure coefficient, b_n . This factor is equal to unity when the level populations follow the Maxwell-Boltzmann law. Under non-LTE conditions, the factor deviates from unity and various statistical processes determine the deviation. The coefficient, β_n (defined in Eqn 2.10) is related to the derivative of b_n with respect to n . β_n has been defined such that a negative value of β_n means that stimulated emission is important whereas a large positive value means that the line will appear in absorption when there is a strong background radiation field. The LTE line optical depth gets modified by the factor $b_n\beta_n$. The calculation of b_n and β_n , parameters that measure the deviation from LTE, thus forms an integral part of the interpretation process and we describe the calculation briefly in this section. The calculation is based on the assumption that the atomic levels are in statistical equilibrium so that the rates of population and depopulation of a level due to various physical processes are equal. This assumption leads to an infinite set of simultaneous equations, one **for** each quantum level n , of the following form which have to be solved to obtain the departure coefficients (Brocklehurst 1970, Dupree 1972, Shaver 1975):

$$N_n \left[\sum_{m < n} A_{n,m} + \sum_m (B_{n,m} I_\nu + C_{n,m}) + C_{n,i} \right] = \sum_{m > n} N_m A_{m,n} + \sum_m N_m (B_{m,n} I_\nu + C_{m,n}) + N_e N_i (\alpha_{i,n} + C_{i,n}) \quad (2.34)$$

where the left hand side represents the rate of depopulation of level, n and the right hand side represents the rate of population of level, n . In the above equation,

- $N_n \sum_{m < n} A_m$ represents the spontaneous emission to lower levels,
- $\sum_{m > n} N_m A_{m,n}$ represents the cascade from higher levels,
- $N_e N_i \alpha_{i,n}$ accounts for radiative recombination,
- $N_n B_{n,m} I_\nu, N_m B_{m,n} I_\nu$ represents induced emission and absorption between adjacent levels ($m = n \pm 1$),
- $N_n C_{n,m}, N_m C_{m,n}$ accounts for collisional transitions to adjacent levels ($m = n \pm 1$),
- $N_n C_{n,i}$ denotes collisional transitions to the continuum,
- $N_e N_i C_{i,n}$ represents three-body recombination.

These are the main physical processes that determine the population, N_n of atoms in a certain level n under typical ISM conditions. The LTE population N_n^* is determined from the Saha equation (Eqn 2.7). The ratio of the two numbers, as mentioned before, is the departure coefficient b_n . At large n ($n > 40$), the different I-states for a certain n are assumed to be statistically populated due to the dominance of I-changing collisional processes (I is the angular momentum quantum number). Hence $b_{nl} = b_n$ (Brocklehurst 1971 and Dupree 1972). In carbon, these I-changing collisions play an important role in making dielectronic-like recombination effective (dielectronic-like recombination is described in the next section).

Various analytical and numerical methods have been developed to estimate N_n from Eqn 2.34. A numerical procedure described by Brocklehurst (1970) has been implemented as a computer code (Salem & Brocklehurst 1979). The departure coefficients are essential in the non-LTE modelling of the observed line strengths and hence the numerical method by Brocklehurst (1970) is described in some detail here.

The infinite system of simultaneous equations for the atomic levels (Eqn 2.34) is truncated at some n_{max} . The solution around $n \sim n_{max}$ is matched to a boundary condition and correction terms are included in the calculation to compensate for the omitted levels, $n > n_{max}$. The resulting system of equations is further reduced by using a matrix condensation technique (Burgess & Summers 1969) where solutions are obtained for only a few 'pivotal' quantum numbers, a subset of n_{max} . The departure coefficients for all the n_{max} levels are then determined using Lagrangian interpolation between the 'pivotal' points. A simplifying assumption regarding the optical depth of Lyman radiation is made, namely either it escapes from the nebula (Case A) or

that it is re-absorbed (Case B). The transparency of the nebula strongly influences the lower- n level populations which are governed primarily by radiative transitions. Generally, Case B can be applied to most nebulae. Salem & Brocklehurst (1979) have computed the departure coefficients and their derivative using 75 pivotal **points** up to a $n_{max} = 500$. The calculations also include the effect of **an** external thermal radiation field on the level populations. These calculations were for a single-electron system *i.e.* hydrogen. Interesting processes **which** modify the level populations can occur in the case of multi-electron atoms. For example, dielectronic-like recombination in carbon atoms is one such process which is effective at temperatures close to 100 K and the next section discusses this process in some detail.

2.6 Dielectronic-like Recombination in Carbon

'Dielectronic **Recombination**', as the name suggests, involves two electrons in the recombination process. This, of course, is possible only in elements heavier than hydrogen. If a free electron with excess kinetic energy is captured in an excited state of **an** atom then the extra energy can be expended in exciting a core electron. In hot ionized **gas** ($T_e \geq 10^4$ K), allowed dipole transitions in core electrons of several electron volts can be excited by a recombining electron, resulting in dielectronic recombination. **Auto-ionization** is the inverse process in which in the absence of any stabilizing mechanism, the recombined electron will be ionized due to radiative deexcitation of the core. But, if a stabilizing mechanism **is** available then this process enhances the level populations at some n , thus **modifying** the line intensities. The process of dielectronic recombination has **been** shown to be important in magnesium, calcium, beryllium and carbon (Shaver 1976) in a low-density, high-temperature ($\sim 10^4$ K) cloud. In low temperature (≤ 50 K) plasma, free electrons are not sufficiently energetic to excite the allowed dipole transitions in the core electrons and hence dielectronic recombination is unimportant. However, in case of the carbon ion, there is a well known fine-structure transition in the ground state, $^2P_{3/2} \rightarrow ^2P_{1/2}$ with an energy of 92 K (0.0079 eV) (Watson, Western, & Christensen 1980, hereafter **WWC80**). As the energy of the fine structure transition is of the order of the kinetic energy of **free** electrons in partially ionized gas at $T_e \sim 100$ K, the electrons can use their excess energies to excite the core fine-structure transition and get captured in the Rydberg states which have negligible binding energies. In this case, auto-ionization is delayed by the 1-changing collisions in the plasma and the Rydberg state is temporarily stabilized. This recombination process is known as 'dielectronic-like recombination'. Dielectronic-like recombination is believed to **signifi-**

cantly influence the level populations in carbon in low- T_e gas.

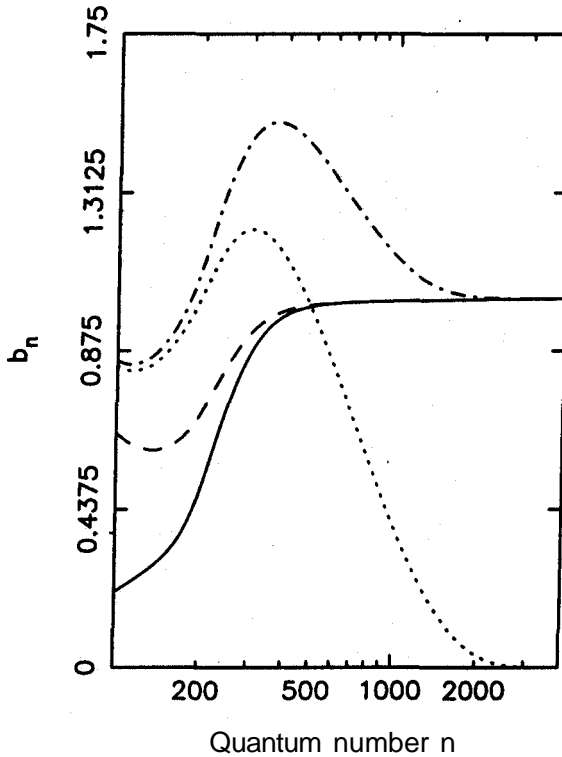


Figure 2.1 The Nature of the Departure Coefficient, b_n . All the curves are for a $T_e = 100$ K, $n_e = 0.1 \text{ cm}^{-3}$, $T_{R100} = 1600$ K and $\alpha = 26$. The solid line represents the variation in the departure coefficient with n if only hydrogenic processes populate the atomic levels, the dashed line is the variation after the inclusion of dielectronic-like recombination but with thermalized fine-structure level population ($R=1$), the dash-dot line is similar to the dashed line except the fine-structure level populations are subthermal ($R \ll 1$). All these three curves are obtained assuming the boundary condition of $b_n \rightarrow 1$ as $n \rightarrow \infty$. The dotted curve traces the variation in b_n with n with the boundary condition $b_n \rightarrow 0$ as $n \rightarrow n_{\text{critical}}$ for dielectronic-like populations and $R \ll 1$ (taken from PAE94).

The salient features of the dielectronic-like capture investigated by WWC80 and Walsinley & Watson (1982) can be summarized as follows.

- The free electrons should have kinetic energies ~ 92 K. This process is, therefore most effective in clouds with temperatures in the range 50 – 200 K.
- The effectiveness of the process depends on the kinetic temperature of free electrons, the relative populations of the fine-structure levels and the I-changing collisions.
- I-changing collisions which convert a Rydberg atom from (n, l) state to (n, l')

state at large- n is the **temporary** stabilizing mechanism against auto-ionization.

- Dielectronic-like recombination may not have a significant effect on the level populations at high density and/or **high kinetic temperature** where the **fine-structure** levels have attained equilibrium populations.

Dielectronic-like recombination manifests itself in different ways depending on the environmental conditions and the principal quantum number. The **effectiveness** of the process depends on the quantity, R , which is the ratio of the non-LTE to the LTE level populations of the fine-structure states (equivalent of b_n) in carbon as given by WWC80 and Ponomarev & Sorochenko (1992).

$$R = \frac{[n(^2P_{3/2})/n(^2P_{1/2})]}{[n(^2P_{3/2})/n(^2P_{1/2})]^*} = \frac{n_e\gamma_e + n_H\gamma_H}{n_e\gamma_e + n_H\gamma_H + A_r} \quad (2.35)$$

where γ_e and γ_H are the de-excitation rates due to collisions with **electrons** and hydrogen atoms respectively. $\gamma_H = 5.8 \times 10^{-10} T_e^{0.02} \text{ cm}^3\text{s}^{-1}$ (Tielens & Hollenbach 1985) and $\gamma_e = 4.51 \times 10^{-6} T_e^{-0.5}$ (Hayes & Nussbaumer 1984). $A_r = 2.4 \times 10^{-6} \text{ s}^{-1}$ is the spontaneous decay rate of $^2P_{3/2} \rightarrow ^2P_{1/2}$. Since dielectronic capture can occur only in ions with a core electron in the lower **fine-structure** state, $^2P_{1/2}$, lower the value of R , **more** effective is the process as shown in Fig 2.1 where **sub-thermal** populations give the dash-dotted curve. For values of R close to unity, the **fine** structure levels have LTE populations and dielectronic-like recombination does not affect the populations significantly (dashed curve in Fig 2.1) and approaches the hydrogenic populations (solid line in Fig 2.1). Small values of R lead to significant effects on the level populations as listed below:

- b_n (dielectronic) $>$ b_n (non-dielectronic) for some combinations of n_e and T_e .
- As shown by the dash-dotted curve in Fig 2.1 for $R = 0.1$, b_n can become larger than unity thus giving **supra-thermal** level populations at those n . With increasing n , collisional interactions with other particles tend to **thermalize** the level populations (also the radiative decay rates and dielectronic processes decrease with increasing n) and $b_n \rightarrow 1$. In hydrogenic calculations, $b_n \leq 1$ with b_n approaching 1 as n increases, hence $d(\ln b_n)/dn > 0$ (Fig 2.1). But in dielectronic-like capture, $b_n > 1$ for some values of the quantum numbers. In this case, b_n has to reduce with increase in n to achieve the asymptotic value of **one**. This leads to negative values for the derivative. When $d(\ln b_n)/dn$ is negative, $\beta_n > 0$ and absorption instead of emission is predicted by dielectronic-like recombination. Although the

hydrogenic computations for b_n also predict absorption lines, the turnover point is at a much higher n (*i.e.* lower frequencies).

- Dielectronic-like capture reduces the derivative $d(\ln b_n)/dn$ for certain n which means a lower negative value for β and hence reduced stimulated emission.

Dielectronic-like recombination involving the **fine-structure** levels in the ground state of carbon is probably an important level populating mechanism in clouds with kinetic temperature near 100 K. The effect is therefore included in all our departure coefficient calculations for carbon.

2.7 Boundary Conditions for calculating Departure Coefficients

Once the statistical processes which **influence** the level populations in an atom are included in the calculations, the departure coefficients till n_{max} can be computed (see **Sec 2.5**). The b_n values near n_{max} are matched with an asymptotic solution which is obtained analytically. The boundary condition is crucial in the calculations, especially for the large n populations. The dash-dotted and dotted curves in Fig 2.1 are the results of two different boundary conditions namely $b_n \rightarrow 1$ as $n \rightarrow \infty$ & $b_n \rightarrow 0$ as $n \rightarrow n_{critical}$. The small- n ($n > 200$) level populations are not **significantly** influenced by the boundary condition as is evident from these two curves. It is not clear which of the two conditions represents the level populations of the high quantum number bound states.

In the boundary condition obtained assuming thermal populations at large- n , the solution is matched with an analytic form of the asymptotic solution $b_n \rightarrow 1$ as $n \rightarrow \infty$ around n_{max} . At large values of n , the atomic radius ($\propto n^2$) become large and collisions are likely to establish LTE populations (*i.e.* $b_n = 1$), even for low-density nebula. The deviations from LTE due to the cutoff at some finite n_{max} was found to be negligible at the n of interest (**Brocklehurst & Seaton 1972, Shaver 1975**), hence the boundary condition $b_n \rightarrow 1$ as $n \rightarrow \infty$ has been used to solve Eqn 2.34. Recently, another line of reasoning has arisen in which the above boundary condition is considered to be non-physical because levels beyond a certain $n_{critical}$ are devoid of bound electrons due to plasma fluctuations in the cloud *i.e.* $N_n = 0$ for $n > n_{critical}$ (**Gulyaev & Nefedov 1989**). The high- n level populations are modified by an extra factor known as the occupation probability of a level ω_n (**Hummer & Mihalas 1988**) so that b_n smoothly decreases to zero *i.e.* $b_n \rightarrow 0$ as $n \rightarrow n_{critical}$. ω_n can be estimated from the atomic or electronic density and the temperature in the gas (**Hummer & Mihalas 1988**). $n_{critical}$ is the highest bound level and is calculated from the electron or atomic density in the

medium. The claim then is that the **correct** boundary condition to apply at the large- n limit is $b_n \rightarrow 0$ as $n \rightarrow n_{\text{critical}}$ (Gulyaev & Nefedov 1989). Presently, it is not clear which of the two boundary conditions is more physical. Knowing that free electrons have $b_n = 1$ and that collisions are supposed to **thermalize** the level populations, the boundary condition $b_n \rightarrow 1$ as $n \rightarrow \infty$ appears to be quite physical. On the other hand, it is true that plasma fluctuations or collisions lead to vanishing of bound levels **beyond** a certain n_{critical} . And hence any boundary condition which **assumes** an infinite number of bound levels has to take this into account. The two boundary conditions predict **different level** populations at the large- n values which are of interest in this work. However, **since** the boundary condition of $b_n \rightarrow 1$ as $n \rightarrow \infty$ appears more physical to us, it is used to calculate the level populations in this thesis.

The original computer code developed by **Brocklehurst & Salem** (1977) for calculating b_n and β_n has been modified over the years to include the effect of more physical **processes** on the level populations and other options. **Walmsley & Watson** (1982) **extended** the **b_n -calculation** to $n_{\text{max}} = 1000$ and included the effect of dielectronic-like recombination process on level populations in carbon. They also modified the code to include the influence of a non-thermal background radiation field on the level populations. **PAE94** extended the b_n - calculations to $n_{\text{max}} = 10000$ by increasing the number of 'pivot' points to 150. They also included an **alternative** boundary condition namely $b_n \rightarrow 0$ as $n \rightarrow n_{\text{critical}}$.

The departure coefficients thus calculated are used to predict the non-LTE intensities over a range of frequencies for the particular physical conditions existing in the nebula. An iterative procedure involving a least squares fit of the predicted intensities to the observed ones is used to estimate the physical conditions in the nebula.

2.8 Interpretation of RRL Observations

The strength, centroid and width of the line are the standard observable parameters of a spectral line. The magnitudes of these observed quantities are dependent on the physical conditions in the emitting cloud. A homogeneous isothermal ionized nebula can be characterized by its temperature, density of **free** electrons and emission measure. The strength and width of a set of recombination lines can, in principle, be interpreted in terms of the temperature and densities at the origin. The Doppler shift of the spectral line can, in most cases, be used to give a **measure** of the distance to the cloud. Unlike optical recombination lines, **RRL** do not suffer attenuation due to dust along the line of sight and thus can be used to probe even optically obscured ionized regions.

In the rest of this section the methods of determining the temperature and density of the ionized gas from the RRL & continuum observations are discussed.

2.8.1 Determination of Electron Temperature

Short descriptions of a few of the methods generally used to estimate the T_e of a nebula from RRL or continuum observations are listed here:

T_e from line to continuum ratio:

If **RRLs** are emitted under conditions close to LTE, then the ratio of the line strength to the thermal radio continuum from the ionized gas can be directly related to the electron temperature of the nebula. This can happen at frequencies where the nebula is optically thin. Hence, if $1 \gg \tau_C \gg \tau_L^*$ (*i.e.* . optically-thin frequencies), then in the absence of a background radiation field, the LTE ratio of the line to continuum brightness temperatures (see Eqn 2.15 and **Eqn** 2.17) is the ratio of the optical depths,

$$\frac{T_l}{T_c} = \frac{\tau_L^*}{\tau_C} \quad (2.36)$$

As the free-free continuum optical depth and the line optical depth have different dependence on the electron temperature, the ratio of the two gives an estimate of the T_e of the nebula. Substituting for the optical depths in the above equation and including the contribution of helium ions to the continuum emission, the LTE electron temperature is given by (Roelfsema & Goss 1992),

$$T_e^* = \left[6943 \nu^{1.1} \frac{1}{(T_l/T_c)} \frac{1}{\Delta V_D} \frac{1}{(1+Y^+)} \right]^{0.87} \text{ K} \quad (2.37)$$

where Y^+ is the relative number abundance of singly-ionized helium. If non-LTE effects are important at the observed frequency, then the above equation is modified by the departure coefficients as follows (Roelfsema & Goss 1992),

$$T_e = T_e^* \left[b_n \left(1 - \frac{2\beta_n}{\tau_C} \right) \right]^{0.87} \text{ K} \quad (2.38)$$

As b_n and β_n also depend on the electron temperature, the use of Eqn 2.38 is not straightforward. Shaver (1980) showed that for any emission measure, EM, there is a unique frequency where the effect of stimulated emission which increases the line strength balances the influence of the continuum optical depth and pressure broadening which decrease the line strength. The line strength under such conditions approaches its LTE value. This frequency ν is given by (Shaver 1980),

$$\nu = 0.081 EM^{0.36} \text{ GHz.} \quad (2.39)$$

At this frequency, the non-LTE corrections to the electron temperature are negligible, i.e. $\frac{T_e}{T_e} \sim 1$. Thus, model dependent departure coefficients need not be calculated and Eqn 2.37 gives the true T_e of the nebula.

T_e from line widths:

At relatively high frequencies (i.e. small values of n), the lines are primarily Doppler-broadened. An upper limit to the kinetic temperature in the cloud can be derived from the width of the spectral line using Eqn 2.23. If the Doppler-broadened RRL from two atomic species coexisting in the nebula can be observed, then the turbulence term in Eqn 2.23 can be eliminated and T_e can be obtained using:

$$T_e = \frac{c^2}{8kln2} \left[\frac{1}{M_1} - \frac{1}{M_2} \right] \left[\left(\frac{\Delta\nu_1}{\nu_1} \right)^2 - \left(\frac{\Delta\nu_2}{\nu_2} \right)^2 \right] \quad (2.40)$$

where

- M_1, M_2 = atomic mass of the two elements
- $\Delta\nu_1, \Delta\nu_2$ = Doppler widths of the two lines
- ν_1, ν_2 = frequency of transition of the two lines.

T_e from observed Brightness Temperature:

At sufficiently low frequencies, HII regions become optically thick and therefore the emergent intensity at these frequencies is close to the blackbody intensity. Any background radiation incident on the cloud is absorbed by the cloud. The observed brightness temperature is related to the electron temperature by,

$$T_b = T_e(1 - e^{-\tau_C}) . \quad (2.41)$$

At frequencies where $\tau_C \gg 1$, the correction factor to T_b is small and $T_b \sim T_e$.

2.8.2 Determination of Electron Density

Electron density can be determined from the following radio observations:

n_e from a pressure-broadened line:

It is obvious from Eqn 2.25 and Eqn 2.27 that with increasing n and n_e , there is a steep rise in the line width due to pressure broadening. The broadening leads to a decrease in the peak line intensity and hence high-sensitivity observations are required to detect the expected Voigt profile from which the true electron density $n_{e,true}$ in the

nebula can be calculated. The widths of the lines from Rydberg atoms is expected to be enhanced by radiation broadening which is also a strong function of n . Separating the contributions of radiation and pressure broadening to the line width requires some additional knowledge such as an estimate of the radiation field surrounding the cloud. If this is not available then the electron density obtained from Eqn 2.27 gives an upper **limit** to $n_{e,true}$.

n_e from modelling the observed line emission:

By definition, lines emitted under LTE conditions **carry** only the information of the electron temperature in the ionized medium. Non-LTE effects in the ionized gas are necessary if the electron density in the medium is to be estimated. In most of the low-density ionized nebulae, non-LTE effects in the form of **inverted** populations and non-thermal populations of the fine-structure levels in carbon are **common** and hence it is possible to estimate the electron density from the observed RRL. The RRL data, preferably covering a wide **frequency** range can be used to obtain the electron temperatures and densities likely to exist at the origin determined using an iterative procedure involving the departure coefficients, b_n and β_n .

n_e from radio continuum:

The average electron density $n_{e,rms}$ in a nebula can be calculated from the optically thin radio continuum brightness if the distance to the source and its angular size are known. This assumes a homogeneous distribution of electrons within the source. The following formula (from **Mezger & Henderson 1967**) is used to determine the electron density :

$$\left(\frac{n_{e,rms}}{cm^{-3}}\right) = u_1 a^{1/2} 6.351 \times 10^2 \left(\frac{T_e}{10^4 K}\right)^{0.175} \left(\frac{\nu}{GHz}\right)^{0.05} \left(\frac{S_\nu}{Jy}\right)^{0.5} \left(\frac{D}{kpc}\right)^{-0.5} \left(\frac{\theta_G}{arcmin}\right)^{-1.5} \quad (2.42)$$

where

- a = ratio of the exact formula (Oster 1961) to the approximate (Altenhoff et al 1960) formula of the continuum optical depth
- u_1 = density distribution model (eg spherical, cylindrical or gaussian)
- S_ν = continuum **flux** density of the source at the frequency ν , Jy
- D = distance to the source, kpc
- $\theta_G = \sqrt{\theta_\alpha \theta_\delta}$, arcmin

The electron density calculated from the continuum **flux** density of an optically thin source is characteristic of the root mean square electron density over the line of sight through the cloud. This is because the flux density depends on the emission measure which is proportional to the square of the electron density. The electron density derived from the width of RRL, on the **otherhand**, is characteristic of the true electron density in the nebula. This is because pressure broadening has a linear dependence on the electron density. If the two are equal then it **suggests homogeneity** in the medium but generally for most ionized regions, $n_{e,rms} \neq n_{e,true}$. The ionized gas is clumpy and **inhomogeneous**. The filling factor measures the volume occupied by matter as compared to the total volume available to it and is quantitatively obtained from the square of the ratio of $n_{e,rms}$ to $n_{e,true}$. Values ranging from *0.01* to 0.5 have been determined for many H II regions and planetary nebulae (**Osterbrock, 1989**).

2.9 Frequency Dependence of Carbon Recombination Lines

A good example of the frequency dependence of line formation, especially at **low**-frequencies, **are** the multi-frequency carbon recombination observations towards Cas A shown in Fig 2.2. The figure, taken from **PAE89**, shows the carbon RRL in the frequency range *34.5–325* MHz. The **RRL** appear in absorption below *115* MHz ($n > 384$) and in emission above *200* MHz ($n < 320$). The phenomenon of turnover from **absorption** to emission with increase in frequency is explained by the relative importance of the radiative and collisional processes acting on the atom that determine the excitation temperature of a level. Another effect seen in Fig 2.2 is that of pressure and radiation broadening which widen the **lines** as the frequency is lowered.

In case of transitions between **large- n** values, typical of a Rydberg atom, the level populations are governed primarily by collisional processes which tend to thermalize the populations, $T_{ex} \sim T_k$. If under such conditions, a strong background radiation field like that of Cas A ($T_{b,100MHz} \sim 2.5 \times 10^7$ K) or the non-thermal Galactic background is present, then the transitions between the high- n levels will appear in absorption against the strong background ($T_{bg} > T_{ex}$). This is clearly observed in the case of Cas A as shown in Fig 2.2.

At lower- n values (which we call intermediate- n), radiative processes dominate the relative populations which lead to inverted populations and negative excitation temperatures *i.e.* non-LTE effects are important. This phenomenon is facilitated by the presence of an external stimulating radiation field. The Einstein coefficient $A \propto 1/n^5$. **Thus, the relatively high- n levels, because of their lower radiative decay rates, get**

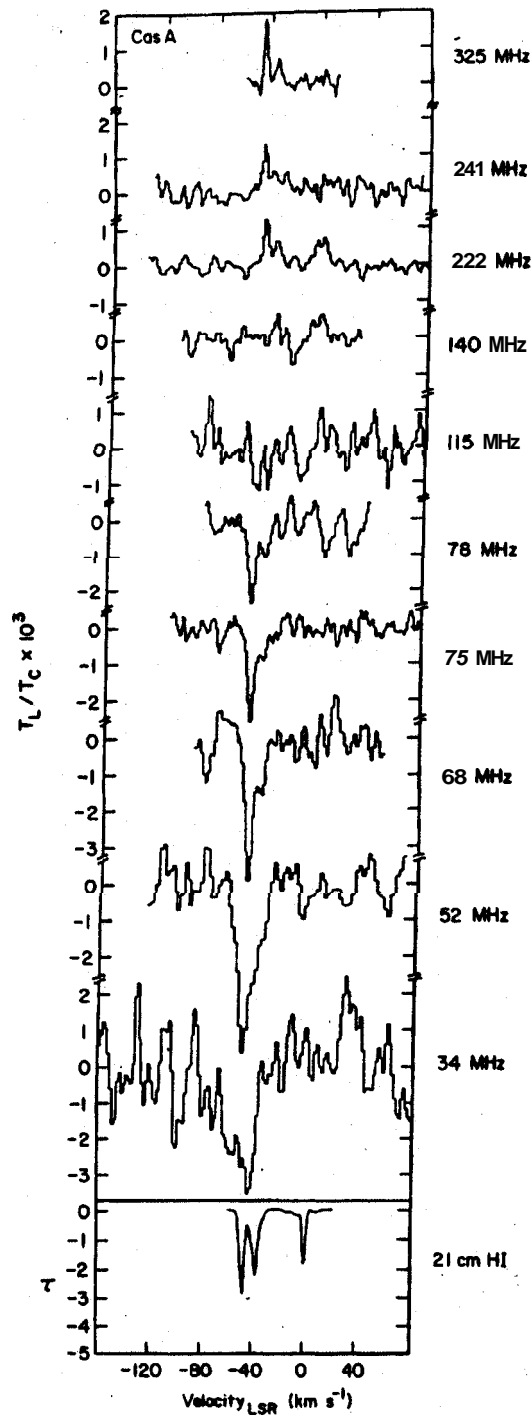


Figure 2.2 Spectra showing carbon recombination lines at frequencies ranging from 325 MHz to 34 MHz arising in the gas in front of Cas A (taken from Payne, Anantharamaiah & Erickson 1989).

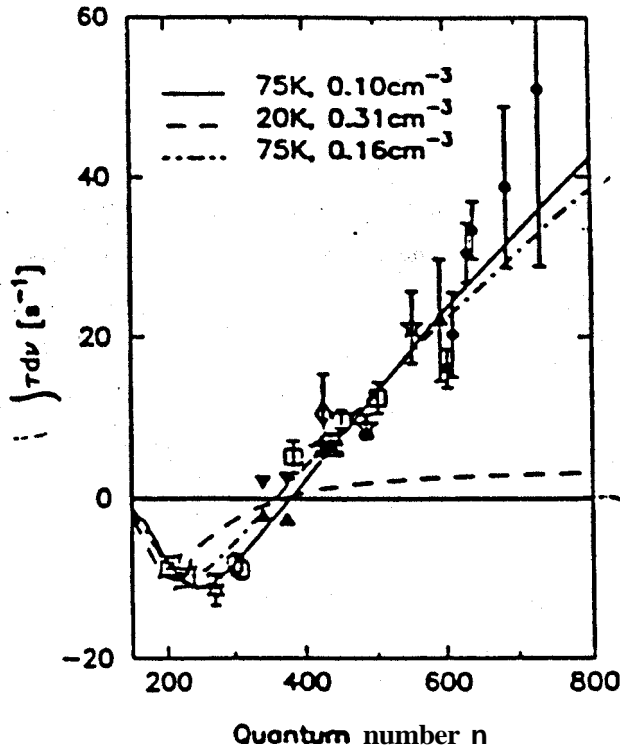


Figure 2.3 Variation in $\int \frac{T_{1d\nu}}{T_{\text{sys}}} d\nu$ of carbon recombination lines with quantum number towards Cas A. The observed data are plotted as points whereas some of the models fitted to this data by Payne, Anantharamaiah & Erickson (1994) are shown superposed as curves.

overpopulated and an inverted population results. The intermediate- n transitions then appear in emission because of stimulated emission by a bright background source. This is clearly seen in the case of Cas A. The turnover from absorption to emission with increasing frequency is bound to be observed in almost all low-density clouds, but the precise frequency at which this happens depends on the details of the physical conditions in the cloud. In the gas in the Perseus arm in the direction towards Cas A, the turnover happens near $n = 350 - 360$. In the high-density clouds (typical of H II regions), large continuum optical depths and pressure broadening prevent the detection of low-frequency RRL and hence this effect. The lines observed towards Cas A are believed to arise in a low-density ($n_e \sim 0.1 \text{ cm}^{-3}$), low-temperature ($T_e \leq 100 \text{ K}$) cloud. The observed integrated optical depth at different quantum number transitions are plotted as points in Fig 2.3 which shows the models found by PAE94. The model fit using the boundary condition $b_n \rightarrow 1$ as $n \rightarrow \infty$ for $T_e = 75 \text{ K}$ and $n_e = 0.1 \text{ cm}^{-3}$ is shown as the solid line in the plot.

2.10 Summary

In this chapter, some theory of radio recombination lines required for interpreting the observations has been presented. Recombination lines, which arise in gas which is in ionization equilibrium, span the electromagnetic spectrum from ultraviolet to radio wavelengths and bring with them information on the physical properties of the region in which they originate. The theory of radiative transfer is used to understand the observed recombination line intensities. These lines are broadened due to various physical processes in the nebula. The resulting profile functions due to thermal & turbulent motions and collisional & radiation broadening are discussed in this chapter. The calculation of departure coefficients which are crucial for determining the **non-LTE level populations** and the process of dielectronic-like **recombination** which modifies level populations in carbon are also briefly described here. Some methods used for determining the temperatures and electron densities of the **line-forming** gas are also described. We end the chapter with a short discussion on the frequency dependence of recombination lines of carbon.